Synchronization of many nanomechanical resonators coupled via a common cavity field

C. A. Holmes, C. P. Meaney, and G. J. Milburn

Centre for Engineered Quantum Systems, School of Mathematical and Physical Sciences, The University of Queensland,
St. Lucia, Queensland 4072, Australia

Using amplitude equations, we show that groups of identical nanomechanical resonators, interacting with a common mode of a cavity microwave field, synchronize to form a single mechanical mode which couples to the cavity with a strength dependent on the squared sum of the individual mechanical-microwave couplings. Classically this system is dominated by periodic behavior which, when analyzed using amplitude equations, can be shown to exhibit multistability. In contrast, groups of sufficiently dissimilar nanomechanical oscillators may lose synchronization and oscillate out of phase at significantly higher amplitudes. Further, the method by which synchronization is lost resembles that for large amplitude forcing which is not of the Kuramoto form.

PACS number(s): 05.45.Xt, 85.85.+j

I. INTRODUCTION

Synchronization of coupled oscillators arises in many different contexts in biology, chemistry, and engineering [1,2]. Such systems show surprising emergent behavior and can be used to encode and process information [3]. In this paper we show how synchronization can arise in arrays of nanomechanical resonators interacting via a common electromagnetic field mode. Recent progress in optomechanical and nanomechanical systems now enables very high frequency mechanical resonators to be coupled strongly to one or more modes of the electromagnetic field in a resonant cavity [4,5]. This is largely driven by a desire to explore the deep quantum domain in which the mechanical resonator is prepared at or near its vibrational ground state [6,7]. As the coupling is essentially nonlinear, the resulting classical dynamics can be complex and must be thoroughly understood if one is to make sense of the quantum phenomenon.

The common feature in these systems is the so-called radiation-pressure coupling, whereby the displacement of each mechanical resonator independently changes the resonance frequency of a common electromagnetic cavity field by an amount proportional to the displacement of each mechanical resonator. This means that there is an effective conservative force acting on each mechanical resonator proportional to the circulating power in the electromagnetic cavity. If the cavity is externally driven, this interaction mediates an indirect all-to-all coupling between each of the mechanical resonators that is highly nonlinear.

If the oscillators are identical, a collective variable can be used to understand the dynamics. In this paper each of the oscillators is a bulk flexural vibrational mode of a mechanical resonator. The resulting set of equations is similar to that considered by Marquardt *et al*. [8], who found that multistability was an important feature of the dynamics for small mechanical damping. Here we are able to derive amplitude equations for the collective variables and use these to map out regions of multistable behavior in the system.

For nonidentical phase oscillators Kuramoto [9] used a collective variable (Kuramoto's order parameter) to characterize the synchronization between the oscillators. More recently the collective dynamics of optomechanical arrays has been described by Heinrich *et al*. [10], who give some

results on synchronization based on a phase model related to Kuramoto's model. Like our model, Ref. [10] is based on the radiation-pressure coupling between the field and mechanical elements. Unlike our model, the mechanical resonators in Ref. [10] interact with a local electromagnetic field mode and are directly coupled by elastic forces. The more complex coupling in our model results in a different mechanism for the loss of synchronization which typically occurs for large amplitude forcing, not small amplitude forcing as occurs in the model of Heinrich *et al*. [10]. Nevertheless, we are able to give specific results on synchronization for two and three mechanical resonators interacting via a common cavity mode and relate these to the behavior of a collective variable, which is related to the cavity field amplitude.

Much of the previous work on synchronized nonlinear oscillators is based on a direct, usually nearest-neighbor, interaction between the individual oscillators, and amplitude equations have been used successfully to analyze the dynamics of such models [11]. We show that amplitude equation methods can also be applied to understand the dynamics of the more complex all-to-all coupling that occurs in our model. Synchronization in coupled microelectromechanical systems has been described [12] and observed [13].

There are at least four kinds of physical implementation of the system discussed here. First, in circuit QED, a coplanar microwave cavity contains the electric field which forms the common field mode. Nanomechanical resonators can then be placed so as to form one plate of a capacitor with the central conductor of the microwave cavity thereby modulating the microwave cavity frequency [14]. Second, at optical rather than microwave frequencies, an optomechanical system can be formed by placing micromechanical dielectric membranes inside the optical cavity [15]. Third, a toroidal optical whispering gallery mode (WGM) cavity is manufactured on a tapered platform raised off a substrate [16]. The mechanical vibrations of the toroid modulate the frequency of the WGM. Finally, optomechanical phononic crystals can be fabricated which are simultaneously photonic crystal lattices to produce localized optical and mechanical modes [17,18].

In the bulk of this paper we will consider a nanomechanical system where a single mode of a superconducting microwave resonator is coupled to the displacements of N
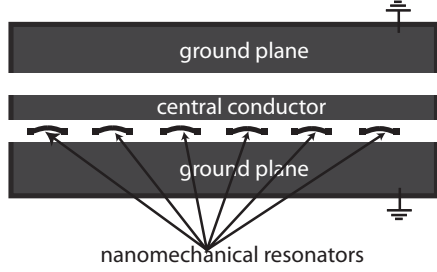
FIG. 1. A schematic of the nanoelectromechanical system under consideration. A superconducting microwave cavity of frequency ω_c mediates a coupling between N nanomechanical resonators capacitively coupled to it. The ith nanomechanical resonator has resonant frequency ω_i and microwave-mechanical coupling strength g_i. The microwave cavity is driven by a linear drive of amplitude ϵ at a detuning from the cavity of δ.

nanomechanical resonators. However, the dynamical model we derive in this section is applicable to other physical implementations in different experimental contexts. In general our model applies to a system of $N + 1$ oscillators: N single flexural modes of independent mechanical resonators whose displacements are coupled to a common single electromagnetic field mode, also modeled as a single simple harmonic oscillator. The coupling between each mechanical resonator and the microwave field in the cavity is capacitive and results in a frequency shift of the cavity resonance frequency that, to lowest order, is proportional to the displacement of the mechanical resonator. This results in a force on each mechanical resonator that is proportional to the intensity of the microwave field in the cavity. This is often called radiation-pressure coupling [19]. A schematic of this system is given in Fig. 1.

We model the dynamics of the microwave field in the co planar transmission line by a lumped circuit LC electrical resonator, and the dynamics of each mechanical resonator is modeled as a single simple harmonic oscillator. The Hamiltonian for a single nanomechanical resonator interacting with the microwave field is

$$\mathcal{H} = \frac{\Phi^2}{2L} + \frac{Q^2}{2C(q)} + v(t)Q + \frac{p^2}{2m} + \frac{m\omega^2}{2}q^2, \quad (1)$$

where the first term is the inductive energy with the Φ the flux through the equivalent inductor with inductance L. The second term is the charging energy with Q the charge on the equivalent capacitor with capacitance $C(q)$, which varies with the displacement of the mechanical element. The third term represents the potential energy due to an external ac bias voltage of the equivalent circuit resonator. The fourth term is the kinetic energy of the mechanical resonator of effective mass m, and the last term is the elastic potential energy of a single flexural mode of the mechanical resonator with ω. As the displacement is small compared to the equilibrium distance between the mechanical resonator and the central conductor of the microwave cavity, we can expand $C(q)$ to linear order in q around the equilibrium displacement q_0 to get an effective Hamiltonian

$$\mathcal{H} = \frac{\Phi^2}{2L} + \frac{Q^2}{2C_0} + \frac{p^2}{2m} + m\omega^2 q^2 + AQ^2 q + v(t)Q, \quad (2)$$

where $C_0 = C(q_0)$ and $A = -\frac{1}{2}\frac{dC(q)}{dq}|_{q=q_0}$. The classical Hamilton equations are

$$\frac{d\Phi}{dt} = \frac{Q}{C_0} + 2AQq + v(t),$$

$$\frac{dQ}{dt} = -\frac{\Phi}{L}, \quad \frac{dq}{dt} = \frac{p}{m}, \quad (3)$$

$$\frac{dp}{dt} = -m\omega^2 q - AQ^2.$$

When $A = 0$, the circuit equations of motion describe simple harmonic oscillation at the frequency

$$\omega_c = \frac{1}{\sqrt{LC_0}}. \quad (4)$$

It is convenient at this point to define dimensionless canonical variables. We do this by first fixing two energy scales, one for the circuit degrees of freedom E_c and one for the mechanical degrees of freedom E_m. The dimensionless canonical variables, (x_c, y_c) for the circuit and (x, y) for the mechanics, are then defined by

$$x_c = \frac{\Phi}{\sqrt{2E_c L}}, \quad y_c = \frac{Q}{\sqrt{2E_c C_0}},$$

$$x = \frac{q}{\sqrt{\frac{2E_m}{m\omega^2}}}, \quad y = \frac{p}{\sqrt{2mE_m}}. \quad (5)$$

We now anticipate an eventual quantum mechanical treatment and set $E_c = \hbar\omega_c$, $E_m = \hbar\omega$. The appearance of $\hbar$ at this stage does not signify anything more than a convenient conversion factor between energy and frequency. We also define a complex amplitude for the circuit degrees of freedom as

$$\alpha = x_c + iy_c, \quad (6)$$

in terms of which we can write the Hamilton equations of motion as

$$\frac{d\alpha}{dt} = -i\omega_c \alpha - ig(\alpha - \alpha^*)x + \mathcal{E}(t),$$

$$\frac{dx}{dt} = \omega y, \quad (7)$$

$$\frac{dy}{dt} = -\omega x - gy_c^2,$$

where

$$g = \frac{\sqrt{2}\,AC_0 E_c}{\sqrt{mE_m}}, \quad \mathcal{E}(t) = \frac{v(t)}{\sqrt{2E_c L}}. \quad (8)$$

We now assume that the circuit is harmonically driven and set

$$\mathcal{E}(t) = \mathcal{E}_0 \sin \omega_D t \quad (9)$$

and define the rotating variable $\bar{\alpha} = \alpha e^{i\omega_D t}$ (equivalent to going to the interaction picture in the quantum description). If we then drop rapidly rotating terms (compared to the time scale of observations), the equations of motion may be approximated by

$$\frac{d\bar{\alpha}}{dt} = -i\delta\bar{\alpha} - ig\bar{\alpha}x - i\epsilon,$$

$$\frac{dx}{dt} = \omega y, \quad (10)$$

$$\frac{dy}{dt} = -\omega x - \frac{g}{2}|\bar{\alpha}|^2,$$

where $\epsilon = -\frac{\mathcal{E}_0}{2}$, and the detuning $\delta = \omega_c - \omega_D$. Noting the time averaged energy of the energy in an *LC* circuit is proportional to $|\alpha|^2$, we see that the effective coupling between the microwave field and the mechanical resonators is described by the effective Hamiltonian $g|\alpha|^2 x$. This form of coupling is often termed radiation-pressure coupling [19]; it is proportional to the circulating power in the cavity field.

We include dissipation of both the microwave field mode and the nanomechanical resonators using the quantum mechanical master equation to incorporate fluctuations correctly. We derive this in Sec. III. There we show that in the classical description the systematic effect of damping (i.e., ignoring fluctuations) change the Hamilton equations to

$$\frac{d\alpha}{dt} = -i\delta\alpha - ig\alpha x - i\epsilon - \kappa\alpha,$$

$$\frac{dx}{dt} = \omega y - \gamma x, \tag{11}$$

$$\frac{dy}{dt} = -\omega x - \frac{g}{2}|\alpha|^2 - \gamma y,$$

where κ and γ are the energy decay rates for the electrical and mechanical energy, respectively, and we have dropped the overbar as from this point on we simply take it for granted that we are working with the rotating variables for the cavity field.

In this paper we are interested in the dynamics of N mechanical resonators interacting with a single mode of the microwave field in the circuit. Assuming a coupling of the form $\sum_i g_i x_i |\alpha|^2$, we see that the equations of motion may be expressed in terms of collective variables:

$$\frac{d\alpha}{dt} = -i\delta\alpha - i\epsilon - i\alpha\sum_{i=1}^{M} N_i X_i - \kappa\alpha,$$

$$\frac{dX_i}{dt} = \omega_i Y_i - \gamma_i X_i, \tag{12}$$

$$\frac{dY_i}{dt} = -\omega_i X_i - \frac{G_i}{2}|\alpha|^2 - \gamma_i Y_i,$$

where X_i, Y_i, and G_i are the M collective combinations

$$X_i = \frac{1}{N_i}\sum_{j\in S_i} g_j x_j, \quad Y_i = \frac{1}{N_i}\sum_{j\in S_i} g_j y_j,$$

$$G_i = \frac{1}{N_i}\sum_{j\in S_i} g_j^2, \tag{13}$$

and S_i are collections of N_i identical nanomechanical oscillators with individual classical positions and momenta x_j and y_j, respectively. We note that the other experimental contexts mentioned in this Introduction can also be described by the same differential equations (12). For example, multiple optomechanical membranes in an optical cavity are described by these equations with different resonant frequencies and coupling strengths [15]. We give a list of the achievable experimental values for various experiments in Table I in the Appendix.

In the following section, we present a detailed analysis of the steady state structure of the nonlinear semiclassical system, including local and global bifurcations. Since the behavior is dominated by oscillatory motion, amplitude equations are derived from which we can obtain specific results about the existence and stability of periodic orbits. It is then a simple step to derive coupled amplitude equations for the case where the mechanical oscillators are not identical, and we analyze two and three coupled oscillator systems. In Sec. III we give a quantum description of the many-body system, and calculate the steady state quantum noise spectra as the first stable limit cycle is approached. Finally, in Sec. IV we summarize our results and suggest new directions for further work.

II. DYNAMICS OF THE CLASSICAL MODEL

Although there are regions of the parameter space where stable critical points exist, periodic motion plays a major role in the dynamics for the cases of both the identical and the nonidentical resonators. If the mechanical resonators are

TABLE I. Raw experimental coupling values for various systems. The "Type" column indicates the experimental context: "S" indicates a superconducting microwave coplanar waveguide resonator ($\hat{a}$) coupled to a nanomechanical resonator ($\hat{b}_i$); "M" indicates an optical cavity ($\hat{a}$) coupled to a micromechanical membrane ($\hat{b}_i$); "T" indicates a toroidal microresonator ($\hat{a}$) coupled to a nanomechanical string resonator ($\hat{b}_i$); and "C" indicates an optomechanical crystal array where an optical mode of a cell ($\hat{a}$) is coupled to a mechanical mode of a cell ($\hat{b}_i$).

Experiment		Mode $\hat{a}$			Mode $\hat{b}_i$		Coupling
Ref.	Type	$\frac{\omega_c}{2\pi}$ (Hz)	$2\frac{\kappa}{2\pi}$ (Hz)	$\frac{|\epsilon|}{2\pi}$ (Hz)	$\frac{\omega_i}{2\pi}$ (Hz)	$2\frac{\gamma_i}{2\pi}$ (Hz)	$\frac{g_i}{2\pi}$ (Hz)
[31]	S	7.49×10^9	$<2.88\times10^6$		1.04×10^6	0.67	866.7×10^{-3}
[22]	S	5.22×10^9	230×10^3	$\lesssim2.145\times10^9$	1.53×10^6	<5.08	190.7×10^{-3}
[14]	S	4×10^9	400×10^3		0.1×10^6	<1	
		$\to10\times10^9$	$\to1\times10^6$		$\to6\times10^6$	$\to<6$	
[14]	S	7.55×10^9	302×10^3		1.41×10^6	<371.1	
[32]	S	$\sim5\times10^9$	490×10^3		2.3×10^6	19.2	49.55×10^{-3}
[23]	S	7.64×10^9	382×10^3	$\lesssim2.434\times10^9$	67×10^6	248.1	25.03
[15]	M	282×10^{12}	4.07×10^6		134×10^3	0.122	27.8
[16]	T		$>4.9\times10^6$		6.5×10^6	65	
					$\to16\times10^6$	$\to1600$	
[16]	T		50×10^6		10.74×10^6	202.64	147.3
[16]	T		50×10^6		8×10^6	200	55.6

identical, even if their couplings are nonidentical, they will synchronize, in phase, to form a single mechanical mode. However the synchronized motion exhibits multi stable behavior. The first two sections, below, discuss the synchronized motion of identical mechanical resonators (14), largely via amplitude equations. If, on the other hand, the mechanical resonators naturally oscillate at different frequencies, desynchronization can occur. To analyze this we consider the synchronization between different frequency groups. The resonators can then be attracted to out-of-phase solutions that oscillate at much greater amplitudes. In the final section we obtain specific results, via coupled amplitude equations, for synchronization between two and three frequency groups.

For all of the bifurcations that occur a scaled version of the cavity forcing ϵ, which is tunable in an experiment, can be thought of as the bifurcation parameter. There are two time scales in the system; the amplitude decay rate κ of the common cavity mode and the decay rate of the resonators, which is an order of magnitude smaller and will be important for the derivation of the amplitude equations. The amplitude decay rate κ of the common cavity mode provides a natural time scale and we introduce a new time parameter $t' = \kappa t$; rescaled nanomechanical variables $X_i' = \frac{X_i}{\kappa}$ and $Y_i' = \frac{Y_i}{\kappa}$; and dimensionless coupling constants $\delta' = \frac{\delta}{\kappa}$, $\epsilon' = \frac{\epsilon}{\kappa}$, $\omega_i' = \frac{\omega_i}{\kappa}$, $\gamma_i' = \frac{\gamma_i}{\kappa}$, $G_i' = \frac{G_i}{\kappa^2}$, and $\bar{\omega}_i' = \sqrt{\omega_i'^2 + \gamma_i'^2}$. This gives

$$\frac{d\alpha}{dt'} = -(1 + i\delta')\alpha - i\alpha \sum_{i=1}^{M} N_i X_i' - i\epsilon',$$

$$\frac{d^2 X_i'}{dt'^2} = -\bar{\omega}_i'^2 X_i' - \frac{G_i' \omega_i'}{2}|\alpha|^2 - 2\gamma_i' \frac{dX_i'}{dt'}. \tag{14}$$

If the uncoupled mechanical resonators are identical ($\omega_1' = \omega'$, $\gamma_1' = \gamma' \Rightarrow \bar{\omega}_1' = \bar{\omega}'$), then the oscillators synchronize. This is a natural consequence of linear damping and the fact that each oscillator experiences the same forcing. Consider $u = X_i' - X_j'$; then $u = 0$ is a stable solution of its equation of motion:

$$\frac{d^2 u}{dt'^2} = -\bar{\omega}^2 u - 2\gamma' \frac{du}{dt'}, \tag{15}$$

provided $\gamma' > 0$.

The synchronized motion can then be represented in collective variables (14) which, suppressing the use of primes, gives the following:

$$\frac{d\alpha}{dt} = -(1 + i\delta)\alpha - i\alpha N X - i\epsilon,$$

$$\frac{d^2 X}{dt^2} = -\bar{\omega}^2 X - \frac{G\omega}{2}|\alpha|^2 - 2\gamma \frac{dX}{dt}. \tag{16}$$

For the remainder of this paper we suppress the uses of primes in the notation, and remind the reader that all couplings are now dimensionless with the cavity decay rate determining the natural time scale of the system.

From a dynamical point of view $\epsilon\sqrt{NG}$ acts as one parameter, and in fact both N and G could be removed by scaling

$$\bar{X} = NX, \quad \bar{\alpha} = \alpha\sqrt{NG}, \quad \bar{\epsilon} = \epsilon\sqrt{NG}. \tag{17}$$

So if the number of resonators is increased, smaller values of the driving are necessary to achieve the same effect.

A. Critical points, bifurcations, and stability

Without forcing, $\epsilon = 0$, the origin is a stable critical point. As the ϵ is increased from zero the critical point moves away from the origin, its position given by the single real root of the cubic

$$2\bar{\omega}^2 X_0[1 + (\delta + NX_0)^2] + G\omega\epsilon^2 = 0, \tag{18}$$

where $\alpha_0 = -\frac{i\epsilon}{1 + i(\delta + NX_0)}$. However, it loses stability on a Hopf bifurcation, creating a periodic orbit, for both $\delta > 0$ (red detuning) and $\delta < 0$ (blue detuning), provided $\gamma > 0$ and small. The dynamics of this periodic motion is the subject of the next section.

For $\delta > 0$ (red detuning) the Hopf curve is a perturbation of that from the $\gamma = 0$ case where $\sqrt{NG}\epsilon = \sqrt{2\delta\bar{\omega}}$. To first order in γ it is given by

$$\epsilon = \epsilon_H(\omega, \delta, \gamma, NG) = \sqrt{\frac{2\omega}{NG}\left(\delta + \gamma\frac{(1+\omega^2)^2}{2\delta\omega^2}\right)}. \tag{19}$$

For $\delta < 0$ (blue detuning) ϵ is of order $\sqrt{\gamma}$:

$$\epsilon = \epsilon_H(\omega, \delta, \gamma, NG) = \sqrt{\frac{\gamma(1+\delta^2)[(\delta^2 - \omega^2 + 1)^2 + 4\omega^2]}{-\delta NG\omega}}. \tag{20}$$

The Hopf bifurcation is subcritical for $\delta < -\sqrt{\frac{8\omega^2+3}{5}}$ (blue detuning), where periodic orbits can exist for $\epsilon < \epsilon_H(\omega, \delta, \gamma, NG)$. In fact many stable limit cycles can exist for some parameter values because of the presence of saddle node bifurcations of limit cycles each creating a stable and unstable pair of limit cycles. This leads to multistable behavior that has been noticed elsewhere [8,20] for similar systems. These bifurcations are shown in Fig. 2 for $\omega = 2$ and $\gamma = 0.001$. The limit cycle bifurcations were produced using the amplitude equations described in the next section; however, similar results can be produced by following the limit cycles numerically using the package MATCONT [21]. For $\delta < 0$ (blue detuning) eight of the saddle node bifurcations of limit cycles are shown, indicating regions where there are 1–8 pairs of stable and unstable periodic orbits. See the caption for specific details. MATCONT indicates that the situation is dynamically more complicated for $\delta > 0$ (red detuning), involving period doubling and regions of chaos.

Although most of this paper is devoted to the case of blue detuning, where $\delta < 0$, it is worth mentioning that for $\delta > \sqrt{3}$ there is a region where three critical points exist given by the roots of the cubic given above. This triangular shaped region

$$\frac{2\bar{\omega}(2\delta + \sqrt{\delta^2 - 3})}{3\sqrt{NG\omega}\sqrt{\delta + \sqrt{\delta^2 - 3}}}$$

$$= \epsilon_{sn+} < \epsilon < \epsilon_{sn-} = \frac{2\bar{\omega}(2\delta - \sqrt{\delta^2 - 3})}{3\sqrt{NG\omega}\sqrt{\delta - \sqrt{\delta^2 - 3}}} \tag{21}$$
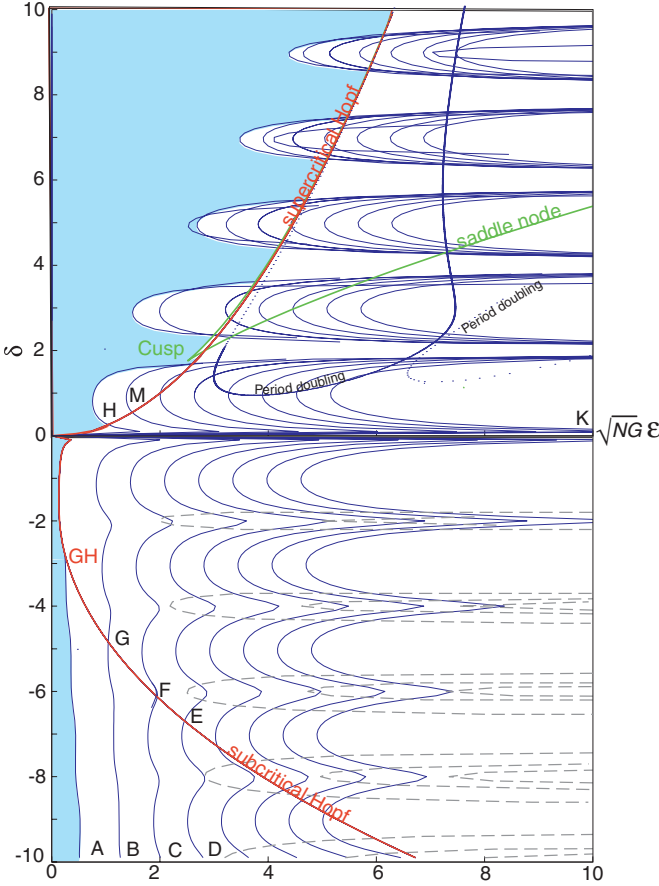
FIG. 2. (Color online) The bifurcation diagram for $\omega = 2$ and $\gamma = 0.001$. In the shaded region there are no periodic orbits and there is one stable critical point. The Hopf bifurcation curve, which is in red, provides a partial boundary of this region. At the generalized Hopf GH (which is at $\delta = \sqrt{7}$ for $\omega = 2$) the Hopf bifurcation changes from super- to subcritical. For $\delta < \sqrt{7}$ the Hopf bifurcation is subcritical and periodic orbits exist to the left of the Hopf curve. Also for $0 < \delta < \sqrt{3}$ there are regions where periodic orbits exist to the left of the Hopf curve. The blue curves A-GH, BGK, CFK, DEK, KHCusp, KMcusp, etc., are saddle node bifurcations of periodic orbits creating a stable and an unstable periodic orbit existing to their right. (Only the first eight are shown.) The lozengelike dashed curves are also saddle node bifurcations of periodic orbits, this time destroying a stable and an unstable periodic orbit. (Once again only a sample are shown.) In the regions ABG(GH) and HMCusp there is one stable critical point and a pair of periodic orbits with opposite stability. In the region G(GH)HK there is one unstable critical point and one stable periodic orbit. In the region BCFG and the region to the left of MCusp there is one stable critical point and two pairs of periodic orbits with opposite stability. In the region FGK there is one unstable critical point and two stable periodic orbits and one unstable periodic orbit. In the region CDEF there is one stable critical point and three stable and three pairs of periodic orbits with opposite stability, etc.

is bounded by ($\epsilon = \epsilon_{sn\pm}$) saddle node bifurcations, shown as green lines in Fig. 2. These intersect in a cusp bifurcation at $\delta = \sqrt{3}$ and $\epsilon\sqrt{NG\omega} = \frac{4\bar{\omega}}{\sqrt{3}}$.

The case $\omega = 2$ is relevant for the experiments described in [8,10]. However, for $\omega > 2$, as in [22,23], there is no qualitative

change in the bifurcation diagram, although the generalized Hopf bifurcation ($\delta = -\sqrt{\frac{8\omega^2+3}{5}}$) occurs for larger values of $|\delta|$. Figure 3 shows the corresponding situation for (a) $\omega = 5$ and (b) $\omega = 10$ and $\gamma = 0.001$ with $\delta < 0$ (blue detuning). Multistable behavior due to the presence of limit cycles stacked above each other remains an important feature (see also Fig. 4).

B. Amplitude equations and multistability for blue detuning ($\delta < 0$)

Periodic orbits and multiple periodic orbits can exist, if the weakly forced oscillators are sufficiently weakly damped. This multistable behavior, resulting from the playoff between weak damping and cavity forcing, has been noted elsewhere [8,10,24]. Here we explore it in more depth using amplitude equations.

The method relies on defining a slow time which is proportional to the damping rate of the resonators ($\tau = \gamma t$) and on assuming that the forcing is on the order of the square root of the damping, $\epsilon = \sqrt{\gamma}\,\bar{\epsilon}$. Then the cavity amplitude is naturally of the same order as the forcing and we can obtain equations for the slowly varying amplitude $A(\tau)$. Let

$$X = X_0 + [A(\tau)e^{i\bar{\omega}t} + \text{c.c.}] = X_0 + 2|A(\tau)|\cos(\bar{\omega}t + \theta),$$
(22)

where X_0 is the critical point of the system given in the previous section, which is $O(\epsilon^2)$. Given that γ is small and both ϵ and $|\alpha|$ are $O(\sqrt{\gamma})$ then $\ddot{X} + \bar{\omega}^2(X - X_0) \approx 2\gamma i\omega\frac{dA}{d\tau}e^{i\bar{\omega}t} + \text{c.c.}$ [25]. The cavity forcing ($\frac{G\omega}{2}|\alpha|^2$) can then be written as a sum of products of Bessel functions. To see this, substitute $X = X_0 + 2|A|\cos(\bar{\omega}t + \theta)$ into the cavity equation;

$$\frac{d\alpha}{dt} = -\{1 + i[\delta + NX_0 + 2N|A|\cos(\bar{\omega}t + \theta)]\}\alpha - i\epsilon.$$
(23)

Then if

$$\alpha = e^{i\psi(t)}\sum_m B_m e^{im\omega t}$$
(24)

it follows that

$$\dot{\alpha} = i\dot{\psi}(t)\alpha + e^{i\psi(t)}\sum_m im\omega B_m e^{im\omega t},$$
(25)

and using the Jacobi Anger expansion [8] $\sum_{n=-\infty}^{\infty} i^n J_n(z) e^{in\theta} = e^{iz\cos\theta}$, this can be matched to the right hand side of the cavity equation if

$$\dot{\psi}(t) = -\frac{2N|A|}{\omega}\cos(\omega t + \theta) \quad \text{and}$$
$$B_m = -\frac{i^{m+1}\epsilon J_m\left(\frac{2N|A|}{\omega}\right)}{\bar{\kappa} + im\omega},$$
(26)

where $\bar{\kappa} = 1 + i(\delta + NX_0)$ and $J_m(x)$ are Bessel functions of the first kind. Substituting this back into

$$\ddot{X} = -\bar{\omega}^2 X - \frac{G\omega}{2}|\alpha|^2 - 2\dot{X}$$
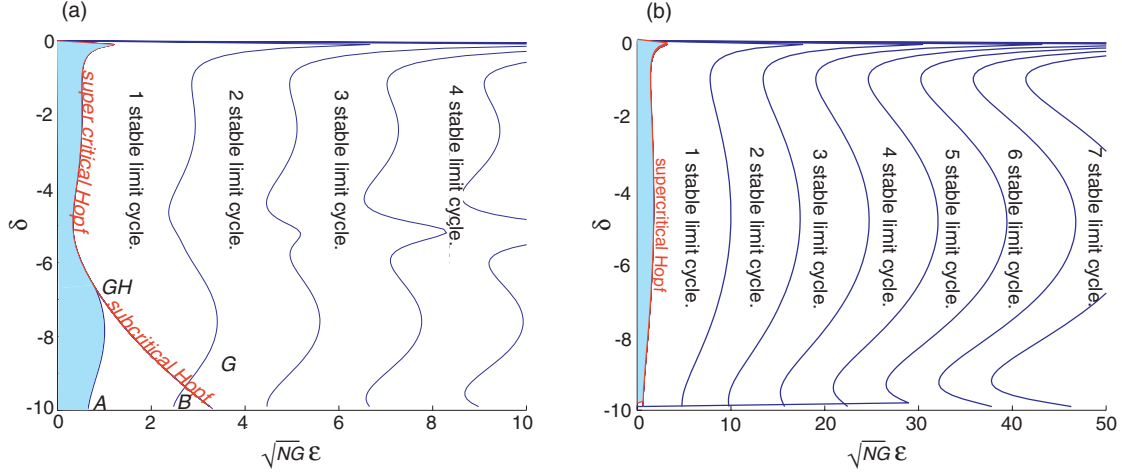(27)

FIG. 3. (Color online) Bifurcation diagrams (a) $\omega = 5$ and (b) $\omega = 10$ and $\gamma = 0.001$ with $\delta < 0$ (blue detuning) showing the Hopf bifurcation (red) and saddle node bifurcations of periodic orbits. The labeling in (a) is similar to that in Fig. 2. For instance, in the region ABG(GH) there is one stable critical point and a pair of periodic orbits with opposite stability.

gives an amplitude equation for the oscillation in terms of sums of pairs of Bessel functions,

$$\frac{dA}{d\tau} = -A - \frac{iG\epsilon^2 e^{i\theta}}{4} \sum_{m=-\infty}^{\infty} \frac{J_m\left(\frac{2N|A|}{\omega}\right) J_{m+1}\left(\frac{2N|A|}{\omega}\right)}{[\bar{\kappa} + i(m+1)\omega](\bar{\kappa}^* - im\omega)}. \tag{28}$$

Identical mechanical resonators synchronize to oscillate with amplitude $A(\tau)$ given by this equation.

In polar form ($A = re^{i\theta}$) the equations become

$$\frac{dr}{d\tau} = -r + G\bar{\epsilon}^2 \sum_{m=0}^{\infty} a_{mr}(\bar{\delta},\omega) J_m\left(\frac{2Nr}{\omega}\right) J_{m+1}\left(\frac{2Nr}{\omega}\right),$$

$$\frac{d\theta}{d\tau} = +\frac{G\bar{\epsilon}^2}{r} \sum_{m=0}^{\infty} a_{mi}(\bar{\delta},\omega) J_m\left(\frac{2Nr}{\omega}\right) J_{m+1}\left(\frac{2Nr}{\omega}\right), \tag{29}$$

where

$$a_{mr}(\bar{\delta},\omega) = \frac{\bar{\delta}\omega^2(2m+1)[1+\bar{\delta}^2+\omega^2 m(m+1)]}{[(1+\bar{\delta}^2-m^2\omega^2)^2+4m^2\omega^2]\{[1+\bar{\delta}^2-(m+1)^2\omega^2]^2+4(m+1)^2\omega^2\}},$$

$$a_{mi}(\bar{\delta},\omega) = \frac{\bar{\delta}\omega(2m+1)\{(1+\bar{\delta}^2-m^2\omega^2)[1+\bar{\delta}^2-(m+1)^2\omega^2]+4m(m+1)\omega^2\}}{2[(1+\bar{\delta}^2-m^2\omega^2)^2+4m^2\omega^2]\{[1+\bar{\delta}^2-(m+1)^2\omega^2]^2+4(m+1)^2\omega^2\}}, \tag{30}$$

and $\bar{\delta} = \delta + X_0$. For $\delta < 0$ (blue detuning) then $X_0 \approx \frac{\gamma[(\delta^2-\omega^2+\kappa^2)^2+4\kappa^2\omega^2]}{2\kappa\omega^2\delta}$. Since each term in the sum has $|A|$ as a factor, the amplitude equation may be rewritten as

$$\frac{dA}{d\tau} = -A + G\bar{\epsilon}^2 NAF(N|A|,\omega,\delta), \tag{31}$$

where $F(Nr,\omega,\delta)$ is a complex function. The conditions for the Hopf bifurcation, given in Sec. II A, can be obtained by setting $\frac{dr}{d\tau} = 0$ in the linearized radial equation,

Since θ does not appear in the equation for r, the periodic orbits of the system are given by

$$F_r(Nr,\omega,\delta) = \frac{1}{r} \sum_{m=0,\infty} a_{mr}(\bar{\delta},\omega) J_m\left(\frac{2Nr}{\omega}\right)$$

$$\times J_{m+1}\left(\frac{2Nr}{\omega}\right) = \frac{1}{NG\bar{\epsilon}^2}. \tag{32}$$

These curves are plotted in Fig. 4 for $\omega = 2$ and $\gamma = 0.01, 0.001, 0.0001$ and various values of δ. Corresponding to

these oscillations, the cavity field amplitude oscillates with frequency $\bar{\omega} + F_i(Nr,\omega,\delta)$ and amplitude $\epsilon\sqrt{2Nr|F|}$:

(Leading oscillatory term in $|\alpha|^2$)

$$= 2Nr\epsilon^2|F(Nr,\omega,\delta)| \cos\{[\bar{\omega} + F_i(Nr,\omega,\delta)]t + \zeta\}, \tag{33}$$

where ζ is a constant.

Although the equation governing the periodic orbits is simple, the multiple ranges of the function $F_r(Nr,\omega,\delta)$, whose contours are plotted in Fig. 6 for $\omega = 2$, result in multistability. Its turning points define the positions of the saddle node bifurcations, which map out the number of periodic orbits existing in parameter space, as shown in Fig. 2. (The curves shown in Fig. 2 were calculated using ten terms in the sum.) Expanded in a Taylor series as a function of r^2 about zero,

$$F_r(Nr,\bar{\kappa},\omega) = F_{r0}(\bar{\kappa},\omega) + r^2 F_{r1}(\bar{\kappa},\omega) + r^4 F_{r2}(\bar{\kappa},\omega) + \cdots, \tag{34}$$
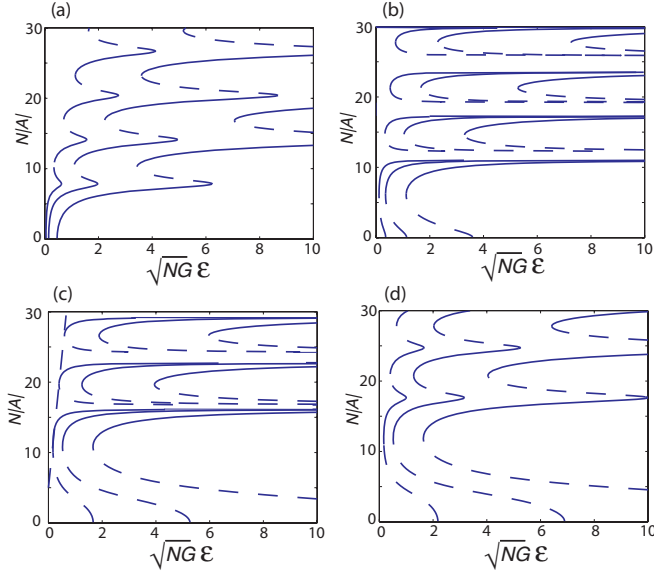
FIG. 4. (Color online) The amplitudes $(N|A| = Nr)$ of the periodic orbits of the system calculated from the amplitude equations as a function of $\sqrt{NG}\epsilon$ for $\omega = 2$ and $\gamma = 0.01, 0.001, 0.0001$ and various values of δ. In (a) $\delta = -2$, (b) $\delta = -5$, (c) $\delta = -9$, and (d) $\delta = -10$. The unstable periodic orbits are given by dashed lines and the stable one are given by solid lines.

FIG. 6. (Color online) The contours of the function $F_r(Nr, \omega, \delta)$ for $\omega = 2$ plotted as a function of (Nr, δ), calculated using 10 terms in the sum of products of Bessel functions. Stable periodic orbits exist in green shaded regions. There are no periodic orbits in the regions enclosed by red lines where $F_r(N|A|, 2, \delta) < 0$.

the linear term $F_{r1}(\bar{\kappa}, \omega)$ defines the criticality of the Hopf bifurcation. The Hopf bifurcation is supercritical, creating a stable periodic orbit, if $F_{r1}(\bar{\kappa}, \omega) < 0$, which is the case here for γ small if $\delta > -\sqrt{\frac{8\omega^2 + 3}{5}}$.

For larger values of ω the oscillations occur at radii with greater values of $N|A| (= Nr)$. Figure 5 compares the amplitudes $|\alpha|$ and $N|A|$ with the bifurcation diagram for $\omega = 10$ and $\gamma = 0.00001$. For instance in the experiment described in [22] the upper bound for the magnitude of ϵ implies that oscillatory behavior occurs for N on the order of 10 and multistable behavior occurs for N on the order of 500.

Here we will not consider the case with $\delta > 0$, which corresponds to red detuning, except to note that the dynamics is more complicated and deserves a separate study. While periodic orbits, similar to those discussed here, exist, there are other orbits as well, associated with the Hopf bifurcation, and many of these undergo period doubling (see Fig. 2) to chaos.

C. *N* nonidentical mechanical resonators and synchronization

If the frequencies and/or dampings of each individual mechanical resonator differ, reduction to a single collective variable is no longer possible. However, the results of the previous section can be generalized to give a set of N
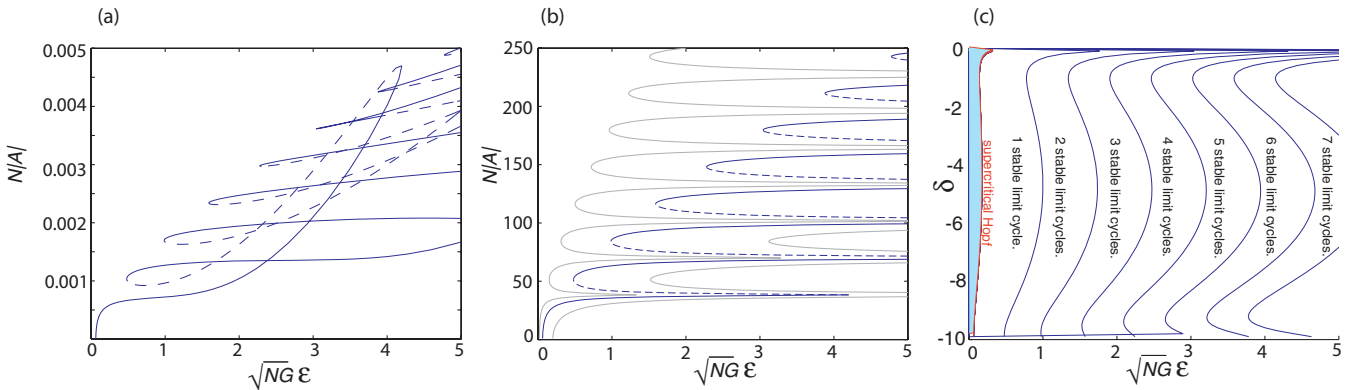

FIG. 5. (Color online) The amplitudes $|\alpha|$ and $N|A|$ as ϵ is increased for $\omega = 10$ and $\gamma = 0.00001$ compared with the saddle node bifurcations that create them. (a) is the cavity amplitude $|\alpha|$, (b) $N|A|$, and (c) the bifurcation diagram.
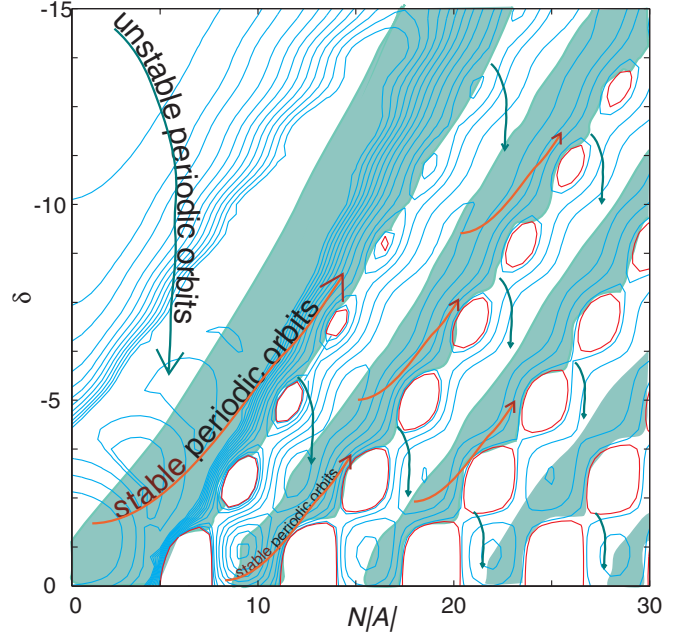
coupled amplitude equations. Here we consider the case where the linear frequencies of the mechanical resonators are approximately the same: $\bar{\omega}_i = \omega + \gamma \Delta \omega_i$. The equations of motion (14) then become

$$\frac{d\alpha}{dt} = -(1 + i\delta)\alpha - i\alpha \sum_i N_i X_i - i\epsilon,$$

$$\ddot{X}_i = -(\omega^2 + 2\omega \Delta \omega_i)X_i - \frac{G_i \omega_i}{2}|\alpha|^2 - 2\gamma \dot{X}_i. \tag{35}$$

As in the previous section, amplitude equations, as functions of a slow time (τ), can be derived for the dominant oscillatory term [11]:

$$X_i = X_0 + [A_i(\tau)e^{i\omega t} + \text{c.c.}] = X_0 + 2|A_i(\tau)| \cos(\omega t + \theta_i). \tag{36}$$

Taking a sum as before and rewriting this as one oscillatory term,

$$X = \frac{1}{N} \sum_i N_i X_i = X_0 + \frac{1}{N}\left(\sum_i A_i(\tau)e^{i\omega t} + \text{c.c.}\right)$$

$$= X_0 + 2|A| \cos(\omega t + \theta), \tag{37}$$

we can see that $|A| = r$ acts as a dynamical order parameter for the mechanical resonators, in the sense of Kuramoto [9],

$$A(\tau) = \frac{1}{N} \sum_i A_i(\tau) \Rightarrow |A| e^{i\theta} = \frac{1}{N} \sum_i r_i e^{i\theta_i}. \tag{38}$$

As before, we can use Bessel functions to work out the cavity amplitude response and substitute this back into the equations for the individual oscillators to give the amplitude

equations,

$$\frac{dA_i}{d\tau} = -(1 + \Delta \omega_i)A_i + N_i G \bar{\epsilon}^2 e^{i\theta} \sum_{m=0,\infty} a_m(\bar{\delta},\omega)$$

$$\times J_m\left(\frac{2N|A|}{\omega}\right) J_{m+1}\left(\frac{2N|A|}{\omega}\right), \tag{39}$$

where $a_m(\bar{\delta},\omega) = a_{mr}(\bar{\delta},\omega) + ia_{mi}(\bar{\delta},\omega)$ is defined in the previous section.

1. Two sets of nonidentical mechanical resonators

In terms of two sets of oscillators this becomes

$$\frac{dA_1}{d\tau} = -(1 + i\Delta \omega_1)A_1 + GN_1 \bar{\epsilon}^2 (A_1 + A_2)F(|A_1 + A_2|),$$

$$\frac{dA_2}{d\tau} = -(1 + i\Delta \omega_2)A_2 + GN_2 \bar{\epsilon}^2 (A_1 + A_2)F(|A_1 + A_2|). \tag{40}$$

If the $\Delta \omega_i$ are equal they do not affect the radial motion and we still have

$$\frac{dr}{d\tau} = -r + G\bar{\epsilon}^2 Nr F_r(Nr,\omega,\delta), \tag{41}$$

which implies that $N^2 r^2 = r_1^2 + r_2^2 + 2r_1 r_2 \cos(\theta_2 - \theta_1)$ is a constant of the motion. Substituting this into the equations for A_i results in a linear system whose symmetrical solution $N_1 A_2 = N_2 A_1$ is stable. So apart from some transients the individual oscillators synchronize, $\frac{d(N_1 A_2 - N_2 A_1)}{dt} = -(\gamma + i\Delta \omega)(N_1 A_2 - N_2 A_1)$, as noted before.

If the $\Delta \omega_i$ are not equal the dynamics of the system, which is a function of the relative phase $\phi = \theta_2 - \theta_1$ only, is given by the nonlinear system

$$\frac{dr_1}{d\tau} = -r_1 + \bar{\epsilon}^2 GN_1\{r_1 F_r(Nr) + r_2[F_r(Nr)\cos\phi - F_i(Nr)\sin\phi]\},$$

$$\frac{dr_2}{d\tau} = -r_2 + \bar{\epsilon}^2 GN_2\{r_2 F_r(Nr) + r_1[F_r(Nr)\cos\phi + F_i(Nr)\sin\phi]\}, \tag{42}$$

$$\frac{d\phi}{d\tau} = \Delta \omega_{21} + \bar{\epsilon}^2 GF_i(Nr)\left[(N_2 - N_1) + \left(\frac{N_2 r_1}{r_2} - \frac{N_1 r_2}{r_1}\right)\cos\phi\right] + \bar{\epsilon}^2 GF_r(Nr)\left(\frac{N_2 r_1}{r_2} + \frac{N_1 r_2}{r_1}\right)\sin\phi,$$

where $F_{i,r}(Nr) = F_{i,r}(Nr,\omega,\delta)$, $Nr = |A_1 + A_2| = \sqrt{r_1^2 + r_2^2 + 2r_1 r_2 \cos\phi}$, and $\Delta \omega_{21} = \Delta \omega_2 - \Delta \omega_1$. For $N_1 = N_2$ we can assume that $\Delta \omega_{21} > 0$ as the transformation ($\Delta \omega_{21} \rightarrow -\Delta \omega_{21}, \phi \rightarrow -\phi$) and ($r_1 \rightarrow r_2$ and vice versa) leaves the equations unchanged. The coupling, however, is strong rather than weak and the system cannot be reduced to a phase model. But it is nevertheless useful to compare our results with those of similar phase and phase amplitude models [2,9,11,26,27].

In the simplest two-oscillator phase model ($\dot{\phi} = \Delta \omega - K \sin\phi$ with $\phi = \theta_2 - \theta_1$) there are two critical points, approximately an in-phase and an out-of-phase solution. One of the critical points is stable, for $|\Delta \omega|$ sufficiently small ($|\Delta \omega| < K$). Unsynchronized motion occurs when the critical points are lost via a saddle node bifurcation ($|\Delta \omega| > K$). More complex

models include a $\sin 2\phi$ term in which case the in-phase solution ($\phi \approx 0$) may lose stability to a stable out-of-phase solution ($\phi \approx \pi$). The model here can also be discussed in terms of the stabilities of in-phase and out-of-phase solutions. However the "unsynchronized behavior" occurs as a transient state, resembling the transient rotational motion of a damped nonlinear pendulum started near to the separatrix of the undamped system. Similar motion has been noted for other systems with multistability [24].

Nonzero $\Delta \omega_{21}$ breaks the symmetry and the in-phase critical points, which are still stable for $\Delta \omega_{21}$ very small, exist only with $r_1 \neq r_2$. Their relative sizes as $|\Delta \omega_{21}|$ is varied are shown in Fig. 7(b). As $|\Delta \omega_{21}|$ is increased they lose stability via a Hopf bifurcation, Fig. 7(a). This creates a stable periodic orbit which does not initially envelope the origin.
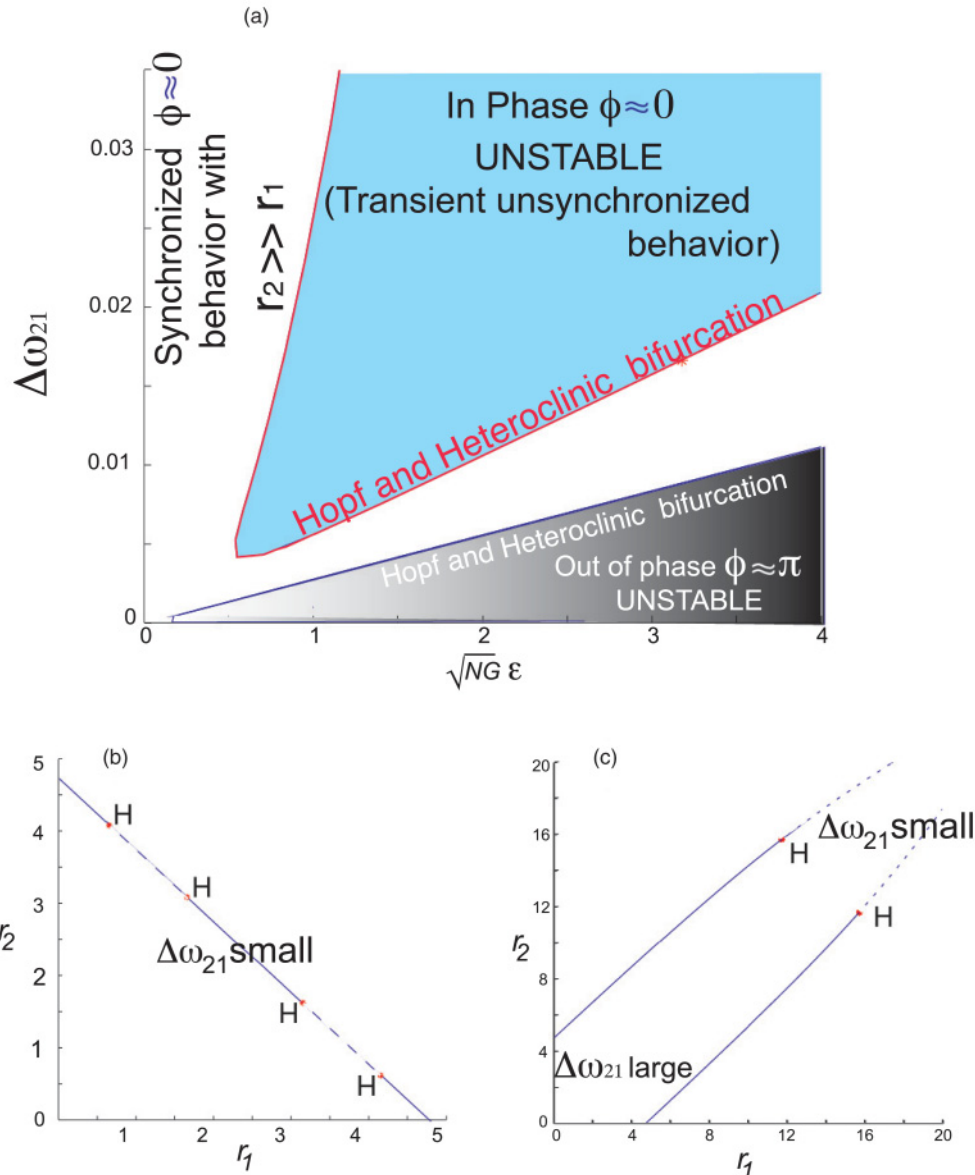
FIG. 7. (Color online) The bifurcation diagram for two mechanical resonators for $N_1 = N_2$, $\gamma = 0.0001$, $\omega = 2$, and $\delta = -1.5$. The in-phase solutions are stable outside the shaded central regions. The out-of-phase solutions are stable outside the slice near the horizontal axis. They are singular at $\Delta\omega_{21} = 0$ and unstable for $|\Delta\omega_{21}|$ small, where they occur for very large values of r_i. In the unshaded regions both in-phase and out-of-phase solutions are stable, but have different basins of attraction. (b) shows the in-phase solution in (r_1,r_2) space as $\Delta\omega_{21}$ is varied. $r_1 + r_2$ remains approximately constant. (c) shows the out-of-phase solution in (r_1,r_2) space as $\Delta\omega_{21}$ is varied.

However, in a bifurcation scenario typical of large amplitude coupling [2], it grows rapidly to enclose the origin. [In (r_1,r_2,ϕ) space this transition is a heteroclinic bifurcation with saddles at $r_{1 \text{ or } 2} = 0$, $\phi = \pm\frac{\pi}{2}$.] Transient unsynchronized motion results for solutions started near the (unstable) in-phase solution, where solutions appear unbounded in phase, but eventually become trapped by a stable out-of-phase solution. [In fact the out-of-phase solutions are only unstable for $\Delta\omega_{21}$ very small, where they exist at large amplitude, Fig. 7(c).] The bifurcation diagram Fig. 7 was created using the package MATCONT with $F(|A|^2, \bar{\kappa}, \omega)$ approximated by the first four terms in its Maclaurin series in $|A|^2$, $N_1 = N_2$, $\gamma = 0.0001$, $\omega = 2$, and $\delta = -1.5$.

If we consider only the solutions started near the in-phase solution then, for sufficiently large $\sqrt{N_1 G}\epsilon > 0.5$, increasing $|\Delta\omega_{21}|$ engenders a loss of synchronization; see Fig. 8. A heteroclinic bifurcation provides the real boundary for loss of synchronization and eventually solutions synchronize into an out-of-phase solution. In the unsynchronized behavior the radii execute fairly large oscillations. However, the oscillations in the cavity amplitude are not large. A typical example is shown in Fig. 8 for $\omega = 2$, $\delta = -1.5$, $\gamma = 0.0001$, $\sqrt{N_1 G}\epsilon = 2$, and $\Delta\omega_{21} = 0.04$ starting near the unstable in-phase solution.

If the N_i are not equal the bifurcation diagram is not symmetrical in $\Delta\omega_{21}$. However, apart from this it is not

dissimilar. The in-phase solution with $\phi = 0$ occurs for $\frac{r_1}{r_2} = \frac{N_1}{N_2}$ and loses stability as $|\Delta\omega_{21}|$ is increased away from zero, eventually stabilizing on an out-of-phase solution.

2. Three sets of nonidentical mechanical resonators

The system for N sets of mechanical resonators,

$$\frac{dr_i}{d\tau} = -r_i + \epsilon^2 N_i G \left[\sum_j r_j [F_r(Nr)\cos(\theta_j - \theta_i) - F_i(Nr)\sin(\theta_j - \theta_i)] \right],$$

$$\frac{d\theta_i}{d\tau} = \Delta\omega_i + \epsilon^2 N_i G \left[\sum_j \frac{r_j}{r_i} [F_i(Nr)\cos(\theta_j - \theta_i) + F_r(Nr)\sin(\theta_j - \theta_i)] \right],$$

(43)

where $(Nr)^2 = |\sum_{i=1}^N A_i|^2 = \sum_{i,j=1}^N r_i r_j \cos(\theta_i - \theta_j)$, may be reduced to $2N - 1$ equations of motion because the equations above are functions only of the relative phase: $\phi_i = \theta_{i+1} - \theta_i$. So three mechanical resonators are described by five equations of motion for $r_1, r_2, r_3, \phi_1, \phi_2$. If the $\Delta\omega_i$ are equal the model can be reduced to that for a single collective variable. In fact, if any two of the $\Delta\omega_i$ are equal then those two resonators can be thought of as one. Using the notation $\Delta\omega_{ij} = \Delta\omega_i - \Delta\omega_j$, the three oscillator case reduces to the two oscillator case if $\Delta\omega_{21} = 0$ or if $\Delta\omega_{32} = 0$ or if $\Delta\omega_{21} + \Delta\omega_{32} = 0$. Figure 9 shows a typical example of loss of synchronization for $\Delta\omega_{21} + \Delta\omega_{32}$ small.

From a dynamical point of view the three resonator case has only one in-phase motion ($\phi_i \approx 0$) and one out-of-phase motion with $\phi_1 \approx \pi$, $\phi_2 \approx 0$ or the other way round. (The case with both $\phi_i \approx \pi$ is dynamically the same as $\phi_1 \approx \pi$, $\phi_2 \approx 0$.) So as before we can think in terms of the in-phase and out-of-phase solutions. (This is not the case for $N \geqslant 4$.) Otherwise

the bifurcation diagram is more complicated, involving two sets of Hopf curves; however, if $\Delta\omega_{31}$ and $\Delta\omega_{32}$ are close the Hopf curves are also close. In contrast, if they differ, as shown in Fig. 10 where we have taken $\Delta\omega_{21} = 5\Delta\omega_{32}$, three unstable regions result. The most complex behavior occurs in the blue region in which the in-phase solution is unstable to both ϕ_i and the motion may switch from librational to rotational motion in one or both of the ϕ_i apparently randomly.

III. QUANTUM MECHANICAL DESCRIPTION

A. Quantum mechanical model

The classical model derived in Sec. I and analyzed in Sec. II is given by the classical Hamiltonian

$$\mathcal{H} = \hbar\delta|\alpha|^2 + \sum_{i=1}^N \hbar\omega_i|\alpha|^2 + \hbar(\epsilon^*\alpha + \epsilon\alpha^*) + \sum_{i=1}^N \hbar g_i|\alpha|^2 x_i,$$
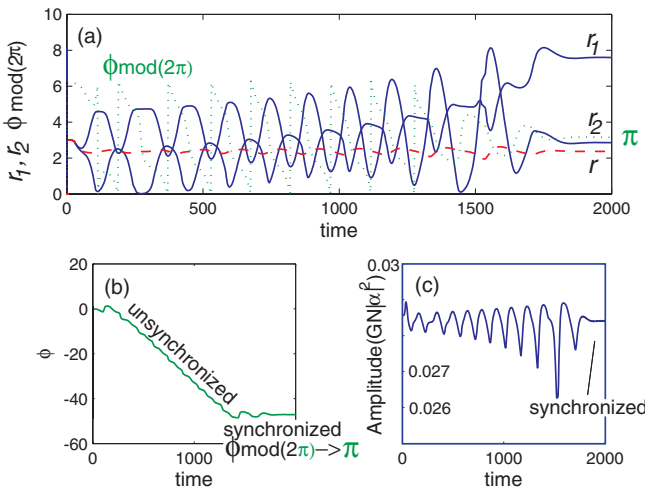
(44)

FIG. 8. (Color online) Transient unsynchronized motion for two nonidentical mechanical resonators for $N_1 = N_2$, $\omega = 2$, $\delta = -1.5$, $\gamma = 0.0001$, $\sqrt{N_1 G}\epsilon = 2$, and $\Delta\omega_{21} = 0.04$. Started near the in-phase solution, in the blue shaded region of Fig. 7, the transient unsynchronized motion is only temporary. Eventually solutions are trapped by an out-of-phase solution [$\phi \mod (2\pi) \to \pi$]. The variables are plotted against time. In (a) r_1 and r_2 are shown in solid lines, the collective variable r is dashed, and $\phi \mod(2\pi)$ is dotted. (b) is a plot of ϕ and (c) is a plot of the amplitude of $GN|\alpha|^2$.

FIG. 9. (Color online) Transient unsynchronized motion of the in-phase solution for three sets of mechanical nonidentical resonators for N_i equal, $\omega = 2$, $\delta = -1.5$, $\gamma = 0.0001$, $\sqrt{N_i G}\epsilon = 2$, $\Delta\omega_{21} = 0.04$, and $\Delta\omega_{21} = 0.045$. Eventually solutions are trapped by an out-of-phase solution [$\phi_i \mod(2\pi) \to \pi$ here]. The variables are plotted against time. In (a) r_i are shown in solid lines, the collective variable r is dashed, and $\phi_i \mod (2\pi)$ are dotted. (b) is a plot of ϕ_i and (c) is a plot of the amplitude of $GN|\alpha|^2$.
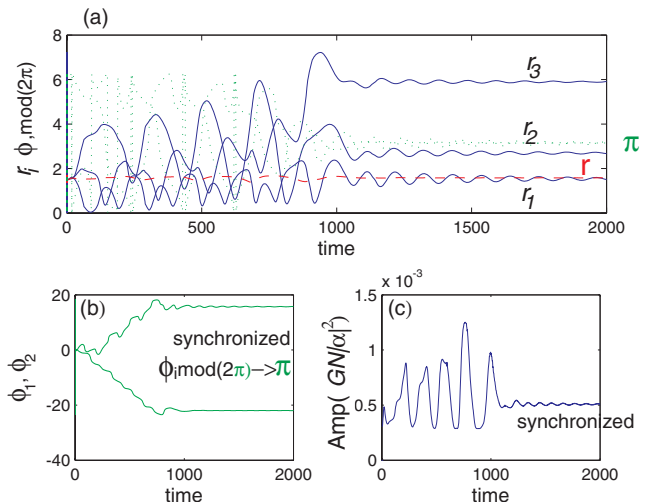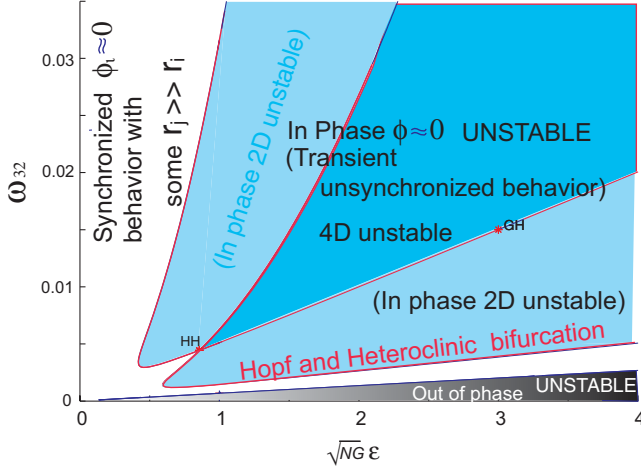
FIG. 10. (Color online) The bifurcation diagram for three mechanical resonators for N_i equal, $\omega = 2$, $\delta = -1.5$, $\gamma = 0.0001$, and $\Delta\omega_{21} = 5\Delta\omega_{32}$. The in-phase solution is stable outside the shaded central regions. The out-of-phase solutions are stable outside the gray regions. In the dark shaded central region the in-phase solution is unstable to both ϕ_1 and ϕ_2 and the motion is transiently unsynchronized, eventually setting on an out-of-phase solution. Once again the out-of-phase solutions tend to exist where at least some of the r_i take larger values.

where the microwave cavity amplitude $\alpha = x_c + iy_c$, and the dimensionless canonical positions x_c and x_i, and their conjugate momenta y_c and y_i, respectively, satisfy the Poisson bracket relations

$$\{x_c, y_c\} = \frac{1}{2\hbar},$$
$$\{x_i, y_j\} = \frac{1}{2\hbar}\delta_{ij}. \tag{45}$$

The original canonical positions $\Phi = \sqrt{2E_c L}\, x_c$ and $q_i = \sqrt{\frac{2E_m}{m\omega^2}}\, x_i$, and their conjugate momenta $Q = \sqrt{2E_c C_0}\, y_c$ and $p_i = \sqrt{2mE_m}\, y_i$ respectively, satisfy the canonical Poisson bracket commutation relations

$$\{\Phi, Q\} = 2\hbar\{x_c, y_c\} = 1,$$
$$\{q_i, p_j\} = 2\hbar\{x_i, y_j\} = \delta_{ij}. \tag{46}$$

The quantum mechanical description of the Hamiltonian dynamics matches that obtained by canonical quantization of the classical Hamiltonian. We promote the canonical position and momenta Φ and Q of the microwave cavity to the quantum mechanical operators $\hat{\Phi}$ and $\hat{Q}$, respectively. Similarly, we promote the nanomechanical resonator positions q_i and momenta p_i to the quantum mechanical operators $\hat{q}_i$ and $\hat{p}_i$, respectively. We then define the annihilation operators for the microwave cavity field mode $\hat{a}$ and the nanomechanical vibrational modes $\hat{b}_i$. We again have the dimensionless microwave cavity quadrature operators $\hat{x}_c = \frac{1}{2}(\hat{a} + \hat{a}^\dagger)$ and $\hat{y}_c = -i\frac{1}{2}(\hat{a} - \hat{a}^\dagger)$, and the dimensionless nanomechanical positions and momenta $\hat{x}_i = \frac{1}{2}(\hat{b}_i + \hat{b}_i^\dagger)$ and $\hat{y}_i = -i\frac{1}{2}(\hat{b}_i - \hat{b}_i^\dagger)$, respectively. We have the commutation

relations for the quantum operators

$$[\hat{a},\hat{a}^\dagger] = \hat{I}, \quad [\hat{x}_c, \hat{y}_c] = i\frac{1}{2}\hat{I}, \quad [\hat{\Phi}, \hat{Q}] = i\hbar\hat{I},$$
$$[\hat{b}_i, \hat{b}_j^\dagger] = \delta_{ij}\hat{I}, \quad [\hat{x}_i, \hat{y}_j] = i\frac{1}{2}\delta_{ij}\hat{I}, \quad [\hat{q}_i, \hat{p}_i] = i\hbar\delta_{ij}\hat{I}, \tag{47}$$

in terms of which the corresponding quantum Hamiltonian in the interaction picture is given by

$$\hat{\mathcal{H}} = \hbar\delta\left(\hat{a}^\dagger\hat{a} + \frac{1}{2}\right) + \sum_{i=1}^{N}\hbar\omega_i\left(\hat{b}_i^\dagger\hat{b}_i + \frac{1}{2}\right)$$
$$+ \hbar(\epsilon^*\hat{a} + \epsilon\hat{a}^\dagger) + \sum_{i=1}^{N}\hbar g_i\left(\hat{a}^\dagger\hat{a} + \frac{1}{2}\right)\hat{x}_i. \tag{48}$$

For a realistic device we adopt a dissipative model. We model both the microwave cavity resonator and the mechanical resonators as being damped in zero-temperature heat baths. This correctly describes the systematic effect of damping but does not include thermal fluctuations. However, we have not included thermal fluctuations in the classical model either. A zero-temperature heat bath for the cavity is certainly justified as the typical microwave cavity is at millikelvin temperature and thus very close to zero [28]. Treating the environment of the N nanomechanical resonators as a zero-temperature heat bath is not a good approximation at typical mechanical frequencies. However, the mean thermal occupation of the ith bath $\bar{n}_i \neq 0$ does not enter the semiclassical equations, and thus the semiclassical bifurcation structure studied in Sec. II is the correct one. The quantum model we are using does describe damping as well as the unavoidable quantum noise arising from spontaneous emission and the uncertainty principle (which enters via the nonpositive definite diffusion matrix discussed below). The amplitude decay for the microwave cavity is κ, and for the ith nanomechanical resonator is γ_i. We then describe the dissipative dynamics with the master equation (with weak damping and the rotating wave approximation for the system-environment couplings)

$$\frac{d\hat{\rho}}{dt} = -\frac{i}{\hbar}[\hat{\mathcal{H}}, \hat{\rho}] + \kappa(2\hat{a}\hat{\rho}\hat{a}^\dagger - \hat{a}^\dagger\hat{a}\hat{\rho} - \hat{\rho}\hat{a}^\dagger\hat{a})$$
$$+ \sum_{i=1}^{N}\gamma_i(2\hat{b}_i\hat{\rho}\hat{b}_i^\dagger - \hat{b}_i^\dagger\hat{b}_i\hat{\rho} - \hat{\rho}\hat{b}_i^\dagger\hat{b}_i), \tag{49}$$

where $\hat{\rho}$ is the density matrix of the coupled system.

Corresponding to the classical description, we are interested in the M collective quantities $\hat{X}_i$ and $\hat{Y}_i$ defined by

$$\hat{X}_i = \frac{1}{N_i}\sum_{j\in S_i} g_j\hat{x}_j,$$
$$\hat{Y}_i = \frac{1}{N_i}\sum_{j\in S_i} g_j\hat{y}_j. \tag{50}$$

We can define creation and annihilation operators for these collective mechanical modes,

$$\hat{B}_i = \frac{1}{N_i}\sum_{j\in S_i} g_j\hat{b}_j,$$
$$\hat{B}_i^\dagger = \frac{1}{N_i}\sum_{j\in S_i} g_j\hat{b}_j^\dagger, \tag{51}$$

where from (47), we can show that the commutation relations for the new collective operators are

$$[\hat{B}_i, \hat{B}_j^\dagger] = \frac{G_i}{N_i}\delta_{i,j}\hat{I}. \tag{52}$$

B. Fokker-Planck-like equation

From the master equation (49), we proceed by deriving a Fokker-Planck-like equation for the nanoelectromechanical system which is the equation of motion of the positive P function $P(\boldsymbol{\chi})$. The positive P function is the Fourier transform of the expectation of the normally ordered characteristic function,

$$P(\boldsymbol{\chi}) = \frac{1}{(2\pi)^{2M+2}}\int \langle e^{i\lambda_{2M+2}\hat{B}_M^\dagger}e^{i\lambda_{2M+1}\hat{B}_M}$$
$$\cdots e^{i\lambda_4 \hat{B}_1^\dagger}e^{i\lambda_3 \hat{B}_1}e^{i\lambda_2 \hat{a}^\dagger}e^{i\lambda_1 \hat{a}}\rangle e^{-i\boldsymbol{\lambda}\cdot\boldsymbol{\chi}}d\boldsymbol{\lambda}, \tag{53}$$

where

$$\boldsymbol{\chi} = [\alpha\beta\mu_1\nu_1\mu_2\nu_2\cdots\mu_M\nu_M]^T,$$
$$\boldsymbol{\lambda} = [\lambda_1\ \lambda_2\ \cdots\ \lambda_{2M+2}]^T. \tag{54}$$

We follow the procedure outlined in [19]. Using the appropriate commutation relations, we arrive at the Fokker-Planck-like equation

$$\frac{dP(\boldsymbol{\chi})}{dt} = -\sum_i \frac{\partial}{\partial\chi_i}[\mathbf{A}(\boldsymbol{\chi})]_i\, P(\boldsymbol{\chi})$$
$$+ \frac{1}{2}\sum_{ij}\frac{\partial}{\partial\chi_i}\frac{\partial}{\partial\chi_j}[\mathbf{B}(\boldsymbol{\chi})\mathbf{B}(\boldsymbol{\chi})^T]_{ij}P(\boldsymbol{\chi}), \tag{55}$$

where the drift term vector $\mathbf{A}(\boldsymbol{\chi})$ is

$$\mathbf{A}(\boldsymbol{\chi}) = \begin{bmatrix} -i\epsilon - (\kappa + i\delta)\alpha - i\frac{1}{2}\alpha\sum_{i=1}^M N_i(\mu_i + \nu_i) \\ i\epsilon - (\kappa - i\delta)\beta + i\frac{1}{2}\beta\sum_{i=1}^M N_i(\mu_i + \nu_i) \\ -(\gamma + i\omega_1)\mu_1 - i\frac{G_1}{2}\alpha\beta \\ -(\gamma - i\omega_1)\nu_1 + i\frac{G_1}{2}\alpha\beta \\ \vdots \\ -(\gamma + i\omega_M)\mu_M - i\frac{G_M}{2}\alpha\beta \\ -(\gamma - i\omega_M)\nu_M + i\frac{G_M}{2}\alpha\beta \end{bmatrix}, \tag{56}$$

and the diffusion term matrix $\mathbf{B}(\boldsymbol{\chi})\mathbf{B}(\boldsymbol{\chi})^T$ is

$$\mathbf{B}(\boldsymbol{\chi})\mathbf{B}(\boldsymbol{\chi})^T$$
$$= \begin{bmatrix} 0 & 0 & -i\frac{G_1}{2}\alpha & 0 & \cdots & -i\frac{G_M}{2}\alpha & 0 \\ 0 & 0 & 0 & i\frac{G_1}{2}\beta & \cdots & 0 & i\frac{G_M}{2}\beta \\ -i\frac{G_1}{2}\alpha & 0 & 0 & 0 & \cdots & 0 & 0 \\ 0 & i\frac{G_1}{2}\beta & 0 & 0 & \cdots & 0 & 0 \\ \vdots & \vdots & \vdots & \vdots & \ddots & \vdots & \vdots \\ -i\frac{G_M}{2}\alpha & 0 & 0 & 0 & \cdots & 0 & 0 \\ 0 & i\frac{G_M}{2}\beta & 0 & 0 & \cdots & 0 & 0 \end{bmatrix}. \tag{57}$$

If we consider only the drift term of the Fokker-Planck-like equation (55) and make the mappings $\beta \mapsto \alpha^*$ and $u \mapsto \nu^*$ to reduce the phase space dimension by half onto the semiclassical phase space (the positive P function has twice the dimensionality of the classical phase space), then we obtain the semiclassical equations of motion.

C. Quantum spectra

A future direction for research that builds on the work of this paper is the investigation of the quantum physics associated with the multistable semiclassical limit cycles. As a starting point, in this section we calculate the linearized spectrum as we increase the driving strength to approach the first Hopf bifurcation at the supercritical Hopf line for blue detuning ($\delta < 0$) in Figs. 2 and 3. We do this calculation for the case of a single group of nanomechanical resonators following the procedure of [29]. For a single group, using the dimensionless notation where we have rescaled the coupling coefficients and time by the cavity dissipation rate κ, we have the stochastic differential equations of motion corresponding to the Fokker-Planck-like equation (55):

$$\frac{d\boldsymbol{\chi}}{dt} = \mathbf{A}(\boldsymbol{\chi}) + \mathbf{B}(\boldsymbol{\chi})\mathbf{E}(t), \tag{58}$$

where

$$\boldsymbol{\chi} = [\alpha\ \beta\ \mu\ \nu]^T, \tag{59}$$

the drift term vector $\mathbf{A}(\boldsymbol{\chi})$ is

$$\mathbf{A}(\boldsymbol{\chi}) = \begin{bmatrix} -(1+i\delta)\alpha - i\frac{1}{2}\alpha N(\mu+\nu) - i\epsilon \\ -(1-i\delta)\beta + i\frac{1}{2}\beta N(\mu+\nu) + i\epsilon \\ -(\gamma+i\omega)\mu - i\frac{G}{2}\alpha\beta \\ -(\gamma-i\omega)\nu + i\frac{G}{2}\alpha\beta \end{bmatrix}, \tag{60}$$

the diffusion term matrix $\mathbf{B}(\boldsymbol{\chi})\mathbf{B}(\boldsymbol{\chi})^T$ is

$$\mathbf{B}(\boldsymbol{\chi})\mathbf{B}(\boldsymbol{\chi})^T = \begin{bmatrix} 0 & 0 & -i\frac{G}{2}\alpha & 0 \\ 0 & 0 & 0 & i\frac{G}{2}\beta \\ -i\frac{G}{2}\alpha & 0 & 0 & 0 \\ 0 & i\frac{G}{2}\beta & 0 & 0 \end{bmatrix}, \tag{61}$$

and $\mathbf{E}(t)$ is the noise process. The principal matrix square root of the diffusion matrix $\mathbf{B}(\boldsymbol{\chi})\mathbf{B}(\boldsymbol{\chi})^T$ is

$$\mathbf{B}(\boldsymbol{\chi}) = \mathbf{B}(\boldsymbol{\chi})^T = \frac{\sqrt{G}}{2}\begin{bmatrix} \sqrt{\alpha} & 0 & -i\sqrt{\alpha} & 0 \\ 0 & \sqrt{\beta} & 0 & i\sqrt{\beta} \\ -i\sqrt{\alpha} & 0 & \sqrt{\alpha} & 0 \\ 0 & i\sqrt{\beta} & 0 & \sqrt{\beta} \end{bmatrix}. \tag{62}$$

The diffusion matrix and its square root have determinants

$$\det\{\mathbf{B}(\boldsymbol{\chi})\mathbf{B}(\boldsymbol{\chi})^T\} = \frac{1}{16}G^4\alpha^2\beta^2,$$
$$\det\{\mathbf{B}(\boldsymbol{\chi})\} = \frac{1}{4}G^2\alpha\beta, \tag{63}$$

and the two matrices are thus positive definite on the semiclassical manifold where $\beta = \alpha^*$. We see that the off-diagonal terms with the factors of i in the matrix square root $\mathbf{B}(\boldsymbol{\chi})$ will take the solution off the semiclassical manifold and will lead to quantum correlations.

We will linearize these equations of motion about the semiclassical fixed points we obtained in Sec. II. In terms of the stochastic differential equations above, we make the mappings $\beta \mapsto \alpha^*$ and $u \mapsto v^*$ to reduce the phase space dimension by half onto the semiclassical phase space (the positive P function has twice the dimensionality of the classical phase space). The

linearized stochastic differential equations are then

$$\frac{d\boldsymbol{\chi}}{dt} \approx \mathbf{M}(\boldsymbol{\chi} - \boldsymbol{\chi}_0) + \mathbf{D}^{1/2}\mathbf{E}(t), \qquad (64)$$

where our Jacobian matrix $\mathbf{M}$ is

$$\mathbf{M} = \frac{\partial \mathbf{f}(\boldsymbol{\chi}_0)}{\partial \boldsymbol{\chi}} = \begin{bmatrix} -(1+i\delta) - i\frac{1}{2}N(\mu_0 + \mu_0^*) & 0 & -i\frac{1}{2}\alpha_0 & -i\frac{1}{2}\alpha_0 \\ 0 & -(1-i\delta) + i\frac{1}{2}N(\mu_0 + \mu_0^*) & i\frac{1}{2}\alpha_0^* & i\frac{1}{2}\alpha_0^* \\ -i\frac{G}{2}\alpha_0^* & -i\frac{G}{2}\alpha_0 & -(\gamma + i\omega) & 0 \\ i\frac{G}{2}\alpha_0^* & i\frac{G}{2}\alpha_0 & 0 & -(\gamma - i\omega) \end{bmatrix}, \qquad (65)$$

$X_0 = \frac{1}{2}(\mu_0 + \mu_0^*)$, and our diffusion matrix about the semiclassical fixed points $\mathbf{D} = \mathbf{B}(\boldsymbol{\chi}_0)\mathbf{B}(\boldsymbol{\chi}_0)^T$ is

$$\mathbf{D} = \begin{bmatrix} 0 & 0 & -i\frac{G}{2}\alpha_0 & 0 \\ 0 & 0 & 0 & i\frac{G}{2}\alpha_0^* \\ -i\frac{G}{2}\alpha_0 & 0 & 0 & 0 \\ 0 & i\frac{G}{2}\alpha_0^* & 0 & 0 \end{bmatrix}. \qquad (66)$$

The linearized normally ordered moments at steady state can be expressed in terms of these matrices [19]

$$\mathbf{S}(\Omega) = \frac{1}{2\pi} \int_{-\infty}^{\infty} e^{-i\Omega\tau} \langle \boldsymbol{\chi}(t)\boldsymbol{\chi}(t+\tau)^T \rangle_{t\to\infty} d\tau$$

$$= \frac{1}{2\pi}(i\Omega\mathbf{I} - \mathbf{M})^{-1}\mathbf{D}(-i\Omega\mathbf{I} - \mathbf{M}^T)^{-1}. \qquad (67)$$

We plot the microwave cavity component of these quantum noise spectra in Fig. 11. We see that in Fig. 11(a) as the Hopf bifurcation is approached, the spectrum becomes more sharply peaked at two frequencies. The frequency corresponding to the Hopf bifurcation—the magnitude of the two purely imaginary eigenvalues—is the peak at the mechanical frequency ω. The

second, shorter but broader peak, is at the detuning δ. For a drive detuned exactly on a sideband, these two peaks coincide. Beyond the supercritical Hopf bifurcation, the semiclassical fixed point is no longer stable and we enter the regime dominated by the first stable limit cycle, where we have the oscillatory motion analyzed by semiclassical amplitude equations in Sec. II. However, we can continue to linearize about this point, and show the results in Fig. 11(b). The two peaks begin to converge as the driving strength and coupling are increased.

The spectra calculated here correspond to the stationary fluctuations in the cavity field. The power spectrum of these fluctuations can be directly measured by homodyne detection. Below the Hopf bifurcation, the noise power spectrum of these fluctuations is peaked at a frequency associated with the decay of fluctuations back to the fixed point. The width of the peaks gives the time scale of this decay. Above the Hopf bifurcation, the fluctuations decay onto the limit cycles. In our model, there are no thermal fluctuations and all fluctuations are due to intrinsic quantum noise manifest as off-diagonal components in the diffusion matrix in (66). Thus the linewidths in the spectra are due only to quantum noise: they would be δ

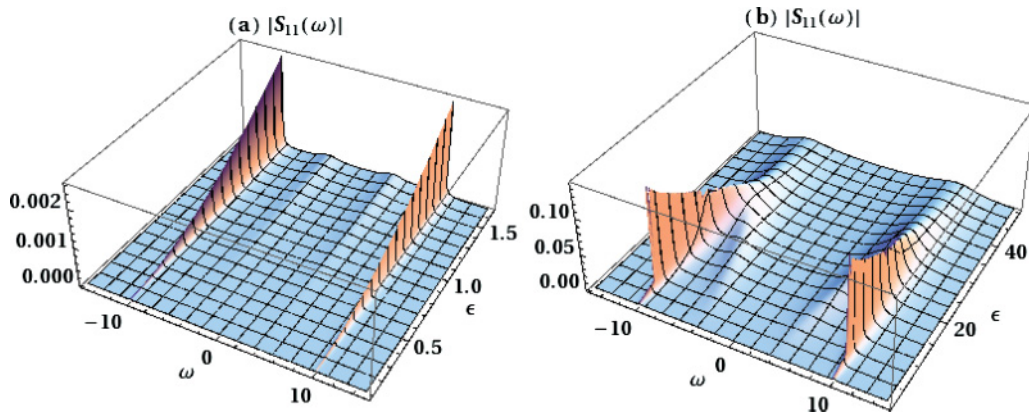
(a) $|S_{11}(\omega)|$ (b) $|S_{11}(\omega)|$

FIG. 11. (Color online) Linearized quantum noise spectrum of the microwave cavity $S_{11}(\Omega)$ (a) approaching the Hopf bifurcation; and (b) continuing the linearization beyond the Hopf bifurcation. The magnitude of the normally ordered cavity spectrum at steady state $(1/2\pi)\int_{-\infty}^{\infty} e^{-i\Omega\tau}\langle\alpha(t)\alpha(t+\tau)^T\rangle_{t\to\infty}d\tau$, the first diagonal element of $\mathbf{S}(\Omega)$, is plotted at the frequency Ω for varying driving amplitude ϵ. Here we have set $\omega = 10$, $\delta = -4$, $\gamma = 0.001$, $N = 1$, $G = 1$, for which the Hopf bifurcation occurs at a driving strength of $\epsilon_h \approx 1.76$.

functions in the classical theory at zero temperature. As such this is a purely quantum feature.

There may be other uniquely quantum features in this model, for example, dissipative switching between fixed points. For example, a system localized on one fixed point (or limit cycle) may show a spontaneous switching to another fixed point (or limit cycle). This is not equivalent to quantum tunneling, neither is it reducible to thermally activated switching, as it occurs in the presence of dissipation at zero temperature. A more careful study is required to determine if the multiple peak structure evident in Fig. 11(b) is evidence for dissipative quantum switching between limit cycles. Such phenomena have been investigated in the case of driven damped parametric amplification in quantum optics [30], which has a similar linearized diffusion matrix to the model of this paper. This will form the subject of a future investigation.

IV. DISCUSSION AND CONCLUSION

We have discussed the situation in which multiple mechanical resonators are coupled to a single mode of the electromagnetic field in a microwave superconducting cavity. This interaction results in an all-to-all coupling between each of the mechanical resonators that is highly nonlinear. However, if the oscillators are identical, they synchronize and a collective variable can be used to understand the dynamics. Analysis of the dynamics of this collective variable (see the bifurcation diagram in Fig. 2) reveals the prevalence of periodic behavior and suggests the use of amplitude equations (28) to describe the dominant oscillation. Even though the amplitude equations involve elliptic functions their overall form is relatively simple for small mechanical damping and from them we are able to gain considerable insight into the dynamics of the collective variable.

The form of the amplitude equations imply the presence of multiple periodic orbits and hysteresis (at the bifurcations of the periodic orbits). Specific results are also easy to extract; for instance, we are able to plot the amplitudes of the mechanical resonators as a function of the external forcing for specific values of the other parameters (Fig. 4) and to locate the saddle node bifurcations of periodic orbits where hysteresis would occur as a result of a slight change in the mechanical forcing (Figs. 2, 3, and 6).

The simplicity of the amplitude equations means that it is straightforward to extend the identical mechanical resonator case to one with distinct subgroups of identical oscillators. Considering two and three frequency subgroups we are able to give bifurcation diagrams showing the regions where synchronization occurs. Synchronization is lost via a mechanism involving a Hopf and heteroclinic bifurcation similar to that found in large amplitude forcing, rather than the sniper bifurcation that is involved in small amplitude forcing and, although in a reduced form, in Kuramoto's phase model. In spite of this difference there is a single collective variable Nr that functions as a measure of synchronized behavior and that is related to a measurable quantity, the cavity amplitude.

Given the current interest in fabricating nanomechanical resonators in microwave cavities, our model offers a realizable

and very controllable way to study synchronization in a system with all-to-all coupling via a common field mode. While the equations for our model cannot be reduced to a simple phase model, it offers some advantages over more complex naturally occurring examples of synchronization. A particularly important feature is that the measured quantity—the cavity field leaving the microwave resonator—has an amplitude that is directly proportional to a collective parameter similar to the order parameter introduced in previous studies of synchronization. The need to use very low temperatures required for superconducting circuits may seem a disadvantage but in fact leads to a huge reduction in noise for both the mechanics and the microwave field. This should lead to especially clean observation of multistability and perhaps even controlled switching between limit cycles. In the long run it also motivates us to study the effect of quantum noise on synchronization, and to look for quantum signatures of synchronization which will be the subject of a future presentation.

APPENDIX: EXPERIMENTAL PARAMETERS

A number of experiments are described by the model examined in this paper,

$$\frac{d\hat{\rho}}{dt} = -\frac{i}{\hbar}[\hat{\mathcal{H}},\hat{\rho}] + \kappa(2\hat{a}\hat{\rho}\hat{a}^\dagger - \hat{a}^\dagger\hat{a}\hat{\rho} - \hat{\rho}\hat{a}^\dagger\hat{a})$$
$$+ \sum_{i=1}^{N} \gamma_i(2\hat{b}_i\hat{\rho}\hat{b}_i^\dagger - \hat{b}_i^\dagger\hat{b}_i\hat{\rho} - \hat{\rho}\hat{b}_i^\dagger\hat{b}_i), \quad \text{(A1)}$$

where

$$\hat{\mathcal{H}} = \hbar\delta\left(\hat{a}^\dagger\hat{a} + \frac{1}{2}\right) + \sum_{i=1}^{N}\hbar\omega_i\left(\hat{b}_i^\dagger\hat{b}_i + \frac{1}{2}\right) + \hbar(\epsilon^*\hat{a} + \epsilon\hat{a}^\dagger)$$
$$+ \sum_{i=1}^{N}\frac{1}{2}\hbar g_i\left(\hat{a}^\dagger\hat{a} + \frac{1}{2}\right)(\hat{b}_i + \hat{b}_i^\dagger), \quad \text{(A2)}$$

and

$$[\hat{a},\hat{a}^\dagger] = \hat{I},$$
$$[\hat{b}_i,\hat{b}_j^\dagger] = \delta_{i,j}\hat{I}. \quad \text{(A3)}$$

A summary of the different values of the parameters for a selection of these experiments is given in Table I. In terms of the dimensionless parameters introduced in Sec. II these become those listed in Table II. Note that the detuning δ is typically set to be on a mechanical frequency sideband, such that $\delta = \omega_i$; and thus while not an experimental limitation, the range of δ we list in the table is $\delta \leqslant \omega_i$. Also note that the maximum driving $|\epsilon|$ indicates the maximum driving before the cavity becomes nonlinear, causing our model to fail. Finally, also note that the factors of 2 in front of κ and γ_i in Table I are present because our κ and γ_i (as defined by the master equation above) are amplitude decay rates, not occupation number decay rates.

TABLE II. Dimensionless experimental coupling values for various systems. The "Type" column indicates the experimental context: "S" indicates a superconducting microwave coplanar waveguide resonator ($\hat{a}$) coupled to a nanomechanical resonator ($\hat{b}_i$); "M" indicates an optical cavity ($\hat{a}$) coupled to a micromechanical membrane ($\hat{b}_i$); "T" indicates a toroidal microresonator ($\hat{a}$) coupled to a nanomechanical string resonator ($\hat{b}_i$); and "C" indicates an optomechanical crystal array where an optical mode of a cell ($\hat{a}$) is coupled to a mechanical mode of a cell ($\hat{b}_i$).

Experiment		Mode $\hat{a}$		Mode $\hat{b}_i$		Coupling
Ref.	Type	$\lvert\delta'\rvert = \frac{\lvert\delta\rvert}{\kappa}$	$\lvert\epsilon'\rvert = \frac{\lvert\epsilon\rvert}{\kappa}$	$\omega_i' = \frac{\omega_i}{\kappa}$	$\gamma_i' = \frac{\gamma_i}{\kappa}$	$g_i' = \frac{g_i}{\kappa}$
[31]	S	$\lesssim 0.722$		0.722	2.33×10^{-7}	6.02×10^{-7}
[22]	S	$\lesssim 13.26$	$\lesssim 1.87 \times 10^4$	13.26	2.209×10^{-5}	1.66×10^{-6}
[14]	S	$\lesssim 0.5$		0.5	2.5×10^{-6}	
		$\rightarrow \lesssim 12$		$\rightarrow 12$	$\rightarrow 6 \times 10^{-6}$	
[14]	S	$\lesssim 9.34$		9.34	1.23×10^{-3}	
[32]	S	$\lesssim 9.39$		9.39	3.92×10^{-5}	2.02×10^{-7}
[23]	S	$\lesssim 350.8$	$\lesssim 1.28 \times 10^4$	350.8	6.5×10^{-4}	1.31×10^{-4}
[15]	M	$\lesssim 0.066$		0.066	3×10^{-8}	1.37×10^{-5}
[16]	T	< 2.65		< 2.65	$< 1.33 \times 10^{-5}$	
		$\rightarrow < 6.53$		$\rightarrow < 6.53$	$\rightarrow < 3.27 \times 10^{-4}$	
[16]	T	$\lesssim 0.43$		0.43	4.05×10^{-6}	5.89×10^{-6}
[16]	T	$\lesssim 0.32$		0.32	4×10^{-6}	2.22×10^{-6}

[1] J. Guckenheimer and D. Holmes, *Nonlinear Oscillations, Dynamical Systems, and Bifurcations of Vector Fields* (Springer-Verlag, Berlin, 1983).

[2] A. Pikovsky, M. Rosenblum, and J. Kurths, *Synchronization: A Universal Concept in Nonlinear Sciences* (Cambridge University, Press, Cambridge, 2003).

[3] G. Orosz, J. Moehlis, and P. Ashwin, Prog. Theor. Phys. **122**, 611 (2009).

[4] T. J. Kippenberg and K. J. Vahala, Science **321**, 1172 (2008).

[5] G. J. Milburn and M. J. Woolley, Contemp. Phys. **49**, 413 (2008).

[6] T. Rocheleau, T. Ndukum, C. Macklin, J. B. Hertzberg, A. A. Clerk, and K. C. Schwab, Nature (London) **463**, 72 (2010).

[7] A. D. O'Connell, M. Hofheinz, M. Ansmann, R. C. Bialczak, M. Lenander, E. Lucero, M. Neeley, D. Sank, H. Wang, M. Weides *et al.*, Nature (London) **464**, 697 (2010).

[8] F. Marquardt, J. G. E. Harris, and S. M. Girvin, Phys. Rev. Lett. **96**, 103901 (2006).

[9] Y. Kuramoto, in *International Symposium on Mathematical Problems in Theoretical Physics*, edited by H. Araki, Lecture Notes in Physics, Vol. 39 (Springer-Verlag, Berlin, 1975), p. 420.

[10] G. Heinrich, M. Ludwig, J. Qian, B. Kubala, and F. Marquardt, Phys. Rev. Lett. **107**, 043603 (2011).

[11] R. Lifshitz and M. C. Cross, in *Review of Nonlinear Dynamics*, edited by H. G. Schuster, Chap. 1, Vol. 1 (Wiley-VCH, Weinheim, 2008).

[12] F. Hoppensteadt and E. Izhikevich, IEEE Trans. Circuits Syst. I **48**, 133 (2002).

[13] M. Zalalutdinov, K. L. Aubin, M. Pandey, A. T. Zehnder, R. H. Rand, H. G. Craighead, J. M. Parpia, and B. H. Houston, Appl. Phys. Lett. **83**, 3281 (2003).

[14] J. D. Teufel, C. A. Regal, and K. W. Lehnert, New J. Phys. **10**, 095002 (2008).

[15] J. D. Thompson, B. M. Zwickl, A. M. Jayich, F. Marquardt, S. M. Girvin, and J. G. E. Harris, Nature (London) **452**, 72 (2008).

[16] G. Anetsberger, O. Arcizet, Q. P. Unterreithmeier, R. Rivière, A. Schliesser, E. M. Weig, J. P. Kotthaus, and T. J. Kippenberg, Nat. Phys. **5**, 909 (2009).

[17] J. Chan, M. Eichenfield, R. Camacho, and O. Painter, Opt. Express **17**, 3802 (2009).

[18] Q. Lin, J. Rosenberg, D. Chang, R. Camacho, M. Eichenfield, K. J. Vahala, and O. Painter, Nat. Photonics **4**, 236 (2010).

[19] D. F. Walls and G. J. Milburn, *Quantum Optics*, 2nd ed. (Springer-Verlag, Berlin, 2008).

[20] A. Dorsel, J. D. McCullen, P. Meystre, E. Vignes, and H. Walther, Phys. Rev. Lett. **51**, 1550 (1983).

[21] W. Govaerts and Y. A. Kuznetsov, computer code MATCONT (2007).

[22] J. D. Teufel, J. W. Harlow, C. A. Regal, and K. W. Lehnert, Phys. Rev. Lett. **101**, 197203 (2008).

[23] J. Sulkko, M. A. Sillanpää, P. Häkkinen, L. Lechner, M. Helle, A. Fefferman, J. Parpia, and P. J. Hakonen, Nano Lett. **10**, 4884 (2010).

[24] F. Mueller, S. Heugel, and L. J. Wang, Phys. Rev. A **77**, 031802 (2008).

[25] P. Glendinning, *Stability, Instability and Chaos: An Introduction to the Theory of Nonlinear Differential Equations* (Cambridge University Press, Cambridge, 1994).

[26] D. Aronson, G. Ermentrout, and N. Kopell, Physica D **41**, 403 (1990).

[27] S. H. Strogatz, Physica D **143**, 1 (2000).

[28] A. Wallraff, D. I. Schuster, A. Blais, L. Frunzio, R.-S. Huang, J. Majer, S. Kumar, S. M. Girvin, and R. J. Schoelkopf, Nature (London) **431**, 162 (2004).

[29] C. A. Holmes and G. J. Milburn, Fortschr. Phys. **57**, 1052 (2009).

[30] P. Kinsler and P. D. Drummond, Phys. Rev. A **43**, 6194 (1991).

[31] J. D. Teufel, T. Donner, M. A. Castellanos-Beltran, J. W. Harlow, and K. W. Lehnert, Nat. Nanotechnol. **4**, 820 (2009).

[32] C. A. Regal, J. D. Teufel, and K. W. Lehnert, Nat. Phys. **4**, 555 (2008).